HHS Public Access

Author manuscript

Sci Transl Med. Author manuscript; available in PMC 2015 September 03.

Published in final edited form as:

Sci Transl Med. 2014 September 3; 6(252): 252ra122. doi:10.1126/scitranslmed.3009332.

Prostate Cancer Cell–Stromal Cell Cross-Talk via FGFR1 Mediates Antitumor Activity of Dovitinib in Bone Metastases

Xinhai Wan[1,†], **Paul G. Corn**[1,†], **Jun Yang**[1], **Nallasivam Palanisamy**[2], **Michael W. Starbuck**[1,3], **Eleni Efstathiou**[1,4], **Elsa M. Li-Ning Tapia**[1], **Amado J. Zurita**[1], **Ana Aparicio**[1],

[*]To whom correspondence should be addressed: nnavone@mdanderson.org.
[†]Denotes equal contributors

LIST OF SUPPLEMENTARY MATERIALS

Materials and methods: FGFR expression and copy number analysis

Fig. S1. *FGFR* gene family expression levels in patient-derived xenografts (PDXs) and the effect of dovitinib on MDA PCa 118b cells growing *in vitro*.

Fig. S2. Effect of 3 weeks of dovitinib treatment on mice bearing MDA PCa 118b cells in the right femurs.

Fig. S3. Effects of 1 day and 2 days of dovitinib treatment on MDA PCa 118b bone tumors.

Fig. S4. Effects of 7 days of dovitinib treatment on the expression of FGFR1, p-FRS2-alpha, p-AKT, and p-MAPK in MDA PCa 118b bone tumors.

Fig. S5. Levels of mouse *Fgfr2IIIc* and *Fgf2* RNA, human *FGFR4* and *FGF9* RNA, and p-MAPK and eIF4E protein in mouse femurs with or without implanted MDA PCa 118b cells.

Fig. S6. Expression of FGFR1 in PCa cells and in tumor-associated osteoblasts in bone biopsy specimens obtained from men in the dovitinib trial at baseline (before treatment).

Table S1. Primer sequences used for RT-PCR

Table S2. Quantitative RT-PCR results.

Table S3. Relative mRNA levels of FGF family members in bone with and without tumors. The mRNA levels were normalized to 10^4 *Gapdh* in tumor-bearing bone (tumor/bone) and contralateral bone

Table S4. Relative mouse *Fgfr1-IIIc* mRNA levels.

Table S5. Relative mRNA levels of FGFR-IIIb and FGFR1-IIIc in MDA PCa 2b tumor-bearing bone

Table S6. Expression of *FGFR1* in prostate and prostate cancer tissues, xenografts, and cell lines

Table S7. Copy number alterations in MDA PCa 118b cells (provided as a separate Excel file)

Table S8. Relative *Fgfr1* mRNA levels in MDA PCa 118b tumor-bearing bone.

Table S9. Growth plate and growth-plate-to-tumor distance in MDA PCa118b tumor-bearing bone.

Table S10. Serum FGF23 levels in MDA PCa 118b tumor-bearing mice treated with vehicle or dovitinib

Table S11. Band intensities on western blot analyses of mice femurs

Table S12. Bone histomorphometric analysis of contralateral (non-tumorous) femurs of mice with MDA PCa 118b bone tumors

Table S13. Micro-CT analysis of femurs of mice treated with vehicle or dovitinib for 4 weeks

Table S14. Tumor volume of MDA PCa 118b tumor-bearing mice assessed by MRI.

Table S15. MDA PCa 118b tumor-bearing mice assessed by DCE-MRI after 7 days dovitinib.

Table S16. Volume of tumor-bearing mice assessed by a T2-weighted fast spin echo MRI after 3 weeks of dovitinib.

Table S17. Characteristics of 34 men enrolled in the dovitinib clinical trial

Table S18. Toxicity events among 34 men enrolled in the dovitinib clinical trial

Table S19. Findings from immunohistochemical analyses of bone biopsies obtained from men in the dovitinib trial at baseline and after 8 weeks of treatment

Author Contribution statement. X.W. and J.Y. designed and performed experiments. P.G.C. and C.J.L. designed the dovitinib clinical trial and P.G.C. collected and analyzed all clinical data. N.P. performed the split-probe analyses; M.W.S. performed bone histomorphometry analyses; E.E. supervised the immunohistochemical analyses; E.M.L.N.T. evaluated findings from immunohistochemical analysis; A.Z. collected and evaluated soluble factors results; A.A. enrolled men into dovitinib study; M.K.R. and V.K. designed, performed, and evaluated the MRI and DCE-MRI studies; E.S.V. participated in the interpretation of the results, manuscript preparation and writing; D.R., Y.W. and X.C. conducted sample preparation and assessment for sequencing; M.L. did bioinformatics analysis; W.M. and F.W. conceived the conceptual framework for analysis and interpretation of FGFR signaling; P.T. performed pathologic evaluation of human and mouse tissue samples; A.M.C. designed and supervised sequencing, copy number and FISH analysis; C.J.L. provided clinical oncological expertise and conceptual insight; N.M.N. provided overall project design, management and supervision, evaluated all results, wrote the manuscript and prepared most of the figures.

Conflict of interest. P.G.C. has served as a paid member of an international advisory board for dovitinib (Novartis). Novartis provided the drug but no funding for this study. C.J.L. has paid advisory and consulting relationships with Astellas, Novartis, BMS, J&J, Pfizer, Excelixis, Medivation, Bayer, Karyopharm, Sanofi. All other authors declare that they have no competing interests.

Materials and data availability. Materials are available through a Material Transfer Agreement and data are freely available.

Murali K. Ravoori[5], **Elba S. Vazquez**[6], **Dan R. Robinson**[2], **Yi-Mi Wu**[2], **Xuhong Cao**[2], **Matthew K. Iyer**[2], **Wallace McKeehan**[8], **Vikas Kundra**[5,7], **Fen Wang**[8], **Patricia Troncoso**[9], **Arul M. Chinnaiyan**[2], **Christopher J. Logothetis**[1], and **Nora M. Navone**[1,*]

[1]Department of Genitourinary Medical Oncology and the David H. Koch Center for Applied Research of Genitourinary Cancers, The University of Texas MD Anderson Cancer Center, Houston, TX 77030

[2]Michigan Center for Translational Pathology, University of Michigan, Ann Arbor, MI 48109

[3]The Rolanette and Berdon Lawrence Bone Disease Program of Texas

[4]University of Athens Greece School of Medicine

[5]Department of Cancer Systems Imaging, The University of Texas MD Anderson Cancer Center, Houston, TX 77030

[6]Department of Biological Chemistry, University of Buenos Aires-National Research Council of Argentina (CONICET-IQUIBICEN), Ciudad Autonoma de Buenos Aires C1428EGA, Argentina

[7]Department of Diagnostic Radiology, The University of Texas MD Anderson Cancer Center, Houston, TX 77030

[8]Center for Cancer and Stem Cell Biology, IBT-Texas A&M Health Science Center, Houston, TX 77030

[9]Department of Pathology, The University of Texas MD Anderson Cancer Center, Houston, TX 77030

Abstract

Bone is the most common site of prostate cancer (PCa) progression to a therapy-resistant, lethal phenotype. We found that blockade of fibroblast growth factor receptors (FGFRs) with the receptor tyrosine kinase inhibitor dovitinib has clinical activity in a subset of men with castration-resistant PCa and bone metastases. Our integrated analyses suggest that FGF signaling mediates a positive feedback loop between PCa cells and bone cells and that blockade of FGFR1 in osteoblasts partially mediates the antitumor activity of dovitinib by improving bone quality and by blocking PCa cell–bone cell interaction. These findings account for clinical observations such as reductions in lesion size and intensity on bone scans, lymph node size, and tumor-specific symptoms without proportional declines in prostate-specific antigen concentration. Our findings suggest that targeting FGFR has therapeutic activity in advanced PCa and provide direction for the development of therapies with FGFR inhibitors.

INTRODUCTION

Bone-forming metastases dominate the clinical picture of men with advanced prostate cancer (PCa), and progression of metastatic lesions in bone is often the initial manifestation of castration-resistant PCa (CRPC) (1, 2). The fibroblast growth factor (FGF)/FGF receptor (FGFR) complex, a signaling axis that typically mediates epithelial–stromal cell interactions, is central to prostate development, is commonly altered during PCa progression, and is integral to normal bone development and function (3, 4).

FGFs are 18 receptor-binding polypeptides that control a broad spectrum of cellular processes via activation of FGFRs in partnership with heparin sulfate (5, 6). FGFR kinase activation is followed by phosphorylation (and therefore activation) of FGFR substrate 2 (FRS2) and recruitment of phospholipase Cγ. FRS2, a single-membrane–anchored adaptor (which has two isoforms, FRS2α and FRS2β), largely mediates FGFR signaling to downstream cascades and networks (such as mitogen-activated protein kinase [MAPK] and protein kinase B [AKT]) (7). Four highly conserved genes (*FGFR1*, *FGFR2*, *FGFR3*, and *FGFR4*) encode alternatively spliced variants of FGFRs that vary in the extracellular ligand-binding and intracellular kinase domains (5, 8). Cell-specific expression of FGFR isoforms and FGF ligands in combination with heparin sulfate motifs confer specificity to intercompartment signaling.

FGFR1- and FGF-mediated epithelial–stromal interactions were implicated in the pathogenesis of PCa in experiments with genetically engineered mouse models (9–11). Correlative observations in clinical specimens have indicated that FGFs or FGFR isoforms are abnormally expressed in human PCa during disease progression (3, 4). Most of these correlative studies were done with tissue samples from primary tumors of men with localized or metastatic disease. Recent studies by our group and others have implicated the FGF axis (in particular FGF9 and FGF8) in the pathogenesis of PCa progression in bone (12, 13) and identified the FGF axis as a candidate target for therapy. To test this, we conducted parallel clinical and preclinical studies of dovitinib (TK1258), a receptor tyrosine kinase inhibitor with potent activity against FGFR and vascular endothelial growth factor receptor (VEGFR), at clinically achievable doses. The results from these studies show that dovitinib is an active therapeutic agent in some men with CRPC and bone metastases and that blockade of FGFR-mediated stromal–epithelial interactions in the bone microenvironment (rather than a direct cytotoxic effect on epithelial cells) has an important role in the antitumor effect. The integration of mouse and human results provides insights into FGF/FGFR biology and into the mechanism underlying the clinical activity that would not have been evident had either model been used in isolation.

RESULTS

Human PCa cells induce mouse *Fgf2* and *Fgfr1* expression in bone

With the goal of modeling the stromal–neoplastic epithelial interactions in bone, we used a human cell line (MDA PCa 2b (14)) and patient-derived xenografts (PDXs) (MDA PCa 118b (13) and MDA PCa 183 (15)) that reflect the biology of PCa progression in bone. The radiographs in Fig. 1A reveal increased density in the femurs injected with PCa cells relative to the hips, indicating that these PCa cells induced a bone reaction. We analyzed tumor-bearing and contralateral sham-injected bones with real-time, reverse-transcription polymerase chain reaction (RT-PCR) using mouse- and human-specific primers (Table S1) to distinguish gene expression in stromal and neoplastic epithelial cells (Table S2). We found that the tumor-bearing femurs had significantly increased expression of mouse *Fgfr1* ($P<0.001$) and *Fgf2* ($P<0.05$) and reduced expression of mouse *Fgfr4* relative to the contralateral femurs in all tumor models tested (Fig. 1B and Table S3). Changes in the expression of other FGF signaling components were inconsistent between models (Fig. 1B

and Table S3). FGFR1 expression in tumor-associated osteoblasts was confirmed by immunohistochemical (IHC) analysis (Fig. 1C). These results indicate that either human PCa cells induce bone cells to express FGFR1 and *Fgf2* or PCa cells recruit bone cells that express FGFR1. We subsequently discovered that in tumor-bearing bones, MDA PCa 118b cells expressed more of the *FGFR1* transcript than MDA PCa 2b and MDA PCa 183 cells (Fig. S1A and Tables S3 and S4).

The specificity of FGFRs for different FGFs is determined by alternative exon usage of the immunoglobulin-like motif of the extracellular domain (4). *FGFR1* encodes two versions of immunoglobulin-like domains in mutually exclusive exons (IIIb and IIIc). Following the same approach as described for Fig. 1B, we used species-specific primers (Tables S1 and S2) and found that the tumor-bearing femurs had significantly increased expression of mouse *Fgfr1-IIIc* compared with the contralateral femurs in all tumor models tested (*P<0.005*) (Fig. 2A and Table S4). Mouse *Fgfr1-IIIb* transcript levels were undetectable by RT-PCR. Analysis of human *FGFR1-IIIb* and *-IIIc* demonstrated that the *FGFR1-IIIc* isoform was expressed at levels between 50 to 100 times higher than the *FGFR1-IIIb* isoform in every PDX examined (Fig. 2B and Table S5). This suggests that FGFR1-IIIc, a high-affinity receptor for FGF1, FGF2 and FGF4, is the prevalent isoform in PCa. Furthermore, *FGFR1-IIIc* transcript levels varied between tumors and correlated with tumor burden (Fig. 2B and C). We subsequently found that MDA PCa 118b cells grown in co-culture with primary mouse osteoblasts (PMOs) (13) expressed more p-FRS2α than when grown alone (Fig. 2D). Together, these results suggest that the FGF axis mediates a positive feedback loop between PCa and bone cells in the tumor microenvironment to promote PCa growth.

FGFR1 is overexpressed in PCa cells and tumor-associated osteoblasts in human PCa bone metastases

We next subjected 183 samples of prostate tissue (28 PCa cell lines and xenograft samples and 155 clinical non-bone samples) to RNA sequencing. We found that the mean expression of *FGFR1* was the highest of all the FGFRs studied (Fig. 3A), with the MDA PCa 118b PDX expressing the most FGFR1 (*z*-score 9.26, $P=1.03e^{-20}$, Fig. 3B). *FGFR1* gene expression varied among the 136 PCa tissue specimens: it ranged from 100 to 200 reads per kilobase per million (RPKMs) in seven samples (5%), 50 to 100 RPKMs in 32 (23%), 20 to 50 RPKM in 63 (46%), and <20 RPKM in 34 specimens (26%). The distribution of *FGFR1* gene expression in the 17 PDXs, 10 PCa cell lines, and 19 tissues samples derived from benign prostate adjacent to PCa was similar to that found in the 136 PCa tissue specimens derived from primary and metastatic non-bone sites (Table S6).

We did not detect *FGFR1* mutations in MDA PCa 118b cells. Copy number analysis from exome sequencing demonstrated high-level focal amplification on chromosome 6, but we found no evidence of focal amplification around the *FGFR1* gene located in a 17.4-Mb region with 2.8 inferred copy number (chr8:21900552-39142362 in Table S7). Finally, split-probe analyses of *FGFR1* assessed by fluorescence in situ hybridization (FISH) identified the presence of two or three copies per cell without any rearrangement or focal amplification

(Fig. 3C). Thus, the high expression of *FGFR1* in MDA PCa 118b cells was not due to genomic rearrangement, copy number aberration, or mutation.

We subsequently assessed FGFR1 expression and cellular localization in human PCa bone metastases (17 specimens from men with CRPC containing >5% tumor cells in each tissue specimen) by IHC analysis. We observed concomitant expression of FGFR1 in both PCa cells and tumor-associated osteoblasts in 2 of 17 cases (12%) (Fig. 3D, **left**). Of the remaining cases, only 8 (53%) had evaluable osteoblasts (the bone tissue had detached in 7 cases as a result of histologic slide preparation); 6 of these 8 (75%) had detectable FGFR1 expression in osteoblasts but not in the tumor cells (Fig. 3D, **middle**). No FGFR1 expression was detected in the remaining 2 cases (Fig. 3D, **right**).

Taken together, these findings support our hypothesis that FGFR1 in PCa cells, osteoblasts, or both participates in a paracrine loop that favors PCa growth in bone and that FGFR1 blockade may represent a rational therapy strategy for men with FGFR1-driven tumors.

Dovitinib has antitumor activity in preclinical models of PCa bone metastases

We selected MDA PCa 118b PDX for further study because it had the highest *FGFR1* expression of the 16 PCa PDXs developed at MD Anderson Cancer Center (Fig. S1A,B). We previously reported that MDA PCa 118b cells and PMOs grow more rapidly in co-culture than alone (13). In this co-culture system, dovitinib reduced the proliferation of PMO and MDA PCa 118b cells, inhibited the FGF9-induced expression of p-FRS2α in PMOs, and reduced endogenous p-FRS2α expression in MDA PCa 118b cells, suggesting that dovitinib specifically blocks FGF signaling in PCa cells and PMOs (Fig. S1C,D).

We next treated mice bearing MDA PCa 118b bone tumors for 3 weeks with low or high dovitinib doses (40 or 60 mg/kg body weight daily) or vehicle. We found that tumor volume (assessed by magnetic resonance imaging [MRI]) was significantly reduced by dovitinib ($P < 0.05$) (Fig. S2A). Micro-computed tomography (CT) analysis of tumor-bearing femurs demonstrated a slight increase in bone mass of the tumor-bearing femur and a reduction in the cortical bone area in the dovitinib-treated mice versus the controls (Fig. S2B).

Dovitinib modulates the FGF axis and induces apoptosis

To investigate how dovitinib modulates FGF signaling, we studied mice bearing MDA PCa 118b bone tumors (Fig. 4A, **top**). Within 7 days of daily treatment with high doses of dovitinib, bone tumors displayed morphologic evidence of cell damage by hematoxylin-and-eosin staining, as well as positive staining for cleaved caspase 3, indicating apoptosis (Fig. 4A, **middle and bottom**). Cell damage was centrally located in the tumor, suggesting that cell death was due to a reduction in trophic support from the surrounding microenvironment (Fig. 4A, **middle and bottom**). Similar findings were observed at earlier time points (Fig. S3). These findings support our hypothesis that the antitumor activity of dovitinib is related at least in part to its modulation of the tumor microenvironment. In line with these findings, no changes in PCa cell expression of FGFR1, p-FRS2, or members of signaling cascades regulated by the FGF axis (p-MAPK and p-AKT) were induced by dovitinib (Fig. S4). However, dovitinib treatment reduced both mouse and human *FGFR1* expression in MDA

PCa 118b bone tumors (Fig. 4B and Table S8), but did not affect mouse *Fgfr2-IIIc* or *Fgf2* nor human *FGFR4* or *FGF9* (Fig. 4B and Fig. S5A).

In an independent 7-day high-dose study, we found that the growth plate and primary and secondary spongiosa were larger in the femurs of dovitinib-treated mice than in controls (Fig. 4C, Table S9). This apparent improvement in bone quality could be a cause or consequence of reduced tumor growth.

Dovitinib blocks FGFR signaling in bone and improves bone quality

We next sought to assess whether dovitinib blocks FGFR signaling in bone. FGF23, an endocrine FGF, is a downstream target of FGFR1 signaling in osteocytes (16). Preclinical and clinical studies of FGFR inhibitors have demonstrated that plasma FGF23 levels initially drop and later increase above basal levels (17–19); elevation of FGF23 plasma levels has been used as a pharmacodynamic biomarker of FGFR inhibition during dovitinib therapy (18, 19). In the current study, FGF23 plasma levels were significantly higher in mice that received 7 days of high dovitinib dose treatment than in vehicle-treated mice (*P=0.0058*) (Fig. 5A, **left and** Table S10). This treatment also resulted in a significant reduction of p-FRS2α (but not p-MAPK) expression in the contralateral non-tumorous bone of tumor-bearing mice (*P=0.0011*) (Fig. 5A, **center and** Table S11, Fig S5). Together these results indicate that dovitinib blocks FGFR signaling in bone cells.

Bone histomorphometric analysis in an independent 7-day dovitinib study revealed a reduced ratio of bone surface to bone volume (P=0.0152) and increased trabecular thickness (P=0.045) in the non-tumorous bone of dovitinib-treated mice compared with control mice (Fig. 5A, **right and** Table S12). These results were confirmed by micro-CT of femurs of non-tumor–bearing male nude mice treated with same dovitinib doses for 4 weeks (Fig. 5B and Table S13).

Dovitinib has antiangiogenic activity

We next examined whether dovitinib's inhibition of VEGFR affects the vasculature, another critical stromal-derived element involved in PCa progression (20, 21). We evaluated tumor volume with T2-weighted fat-saturated (T2-FS) MRI and assessed the vasculature with dynamic contrast-enhanced (DCE)-MRI, which is normally used to assess antiangiogenic therapies in patients and animal models (22). After 7 days of dovitinib treatment, tumor volumes had decreased relative to baseline. T2-FS MRI revealed significant differences between dovitinib-treated and vehicle-treated controls (P<0.05) (Fig. 6A **left and** Table S14). In addition, tumor contrast enhancement (where dark indicates less angiogenesis and bright means more angiogenesis) was significantly lower in mice treated with dovitinib than in controls (P≤0.001) (Fig. 6B **right and** Table S15). These results indicate that the antitumor effect of dovitinib may be partially explained by antiangiogenic activity.

Dovitinib antitumor activity is associated with FGFR expression in PCa PDXs

To test whether dovitinib antitumor activity was the same regardless of FGFR1 expression in PCa cells, we used MDA PCa 118b and MDA PCa 183 PDXs, which reflect the variety of high and low FGFR1 expression found in men with PCa (Fig 3A and B). MDA PCa 118b

expresses 428 RPKM FGFR1, 3 FGFR2, 8 FGFR3, and 0.8 FGFR4. MDA PCa 183 expresses 32 FGFR1, 0.4 FGFR2, 0.7 FGFR3, and 0.7 FGFR4.

After 3 weeks' treatment with low-dose dovitinib, tumor volume in mice bearing MDA PCa 118b bone tumors was significantly smaller than that in vehicle-treated mice (P=0.0004), but tumor volume was not significantly different in mice bearing MDA PCa 183 bone tumors relative to controls (Fig. 7 and Table S16). These results, together with our findings that PMOs induce PCa cells to express p-FRS2α (Fig. 2D), suggest that the effect of dovitinib in the tumor microenvironment alone is not sufficient to mediate its antitumor activity and that activation of FGFR-mediated signaling in PCa cells is an important determinant of dovitinib antitumor activity.

Dovitinib has clinical activity in patients with advanced metastatic CRPC and bone metastases

Given this preclinical evidence of dovitinib's antitumor activity, we conducted a proof-of-principle study of dovitinib in men with CRPC and bone metastases (Table S17). Thirty-four patients have been enrolled to date, and 23 were evaluable for response (completed ≥1 cycle of therapy). Six men (26%) experienced improvements in bone scans (1 with resolution of visible bone metastases and 3 with partial responses on conventional bone scans) or soft-tissue metastases (2 partial responses) at 8 weeks, with a median treatment duration of 19.9 weeks (range 10–35 weeks); 13 patients (57%) experienced stable disease at 8 weeks, with a median treatment duration of 11.7 weeks (range, 6–31 weeks). Four patients (17%) experienced disease progression as best response (Table 1 and Fig. 8A,B). Responding patients generally achieved meaningful reduction of skeletal-associated pain. Most toxicities were grade 1 or 2, and no grade 4 toxicities were noted (Table S18).

Dovitinib targets the tumor microenvironment in CRPC and bone metastases

We analyzed circulating biomarkers reflecting the activity of cancer cells (prostate-specific antigen [PSA]) and bone cells including osteoblasts (bone-specific alkaline phosphatase [BAP]) and osteoclasts (urinary N-terminal telopeptides [uNTx]). Reductions in PSA occurred in 9 of 20 patients (45%) (median change −28%, range −11% to −100%), BAP in 8 of 18 (44%) (median change −21%, range −3% to −54%), and uNTx in 12 of 19 (63%) (median change −18%, range −5% to −69%) (Fig. 8C–E). Of these biomarkers, only the reduction in BAP correlated with longer median duration of treatment (23.6 vs. 10.6 weeks, P=0.056 by Wilcoxon rank-sum test). (Fig. 8E). Duration of treatment is considered a good indication of treatment efficacy because in this study dovitinib treatment was continued until disease progression, unacceptable toxicity, or withdrawal of consent. Thus, reduction of BAP could be associated with treatment efficacy. Consistent with our preclinical studies, these findings demonstrate that dovitinib can modulate both the epithelial and stromal compartments in PCa bone metastases.

We also found an increase in soluble VEGF in 8 of 16 patients (50%) (median change 31%, range 10% to 97%), whereas reductions in soluble VEGFR2 occurred in 12 of 16 (75%) (median change −20%, range −5% to −85%) (Fig. 8F). These results are consistent with dovitinib targeting the VEGF signaling pathway (23).

Finally, pretreatment bone marrow biopsies had >5% PCa tumor infiltration in 16 of 31 patients (52%). FGFR1 expression was observed by IHC analysis in PCa cells from 4 of 16 samples (25%), and 11 of 16 specimens (69%) also contained tumor-associated osteoblasts (Fig. S6). Of the 11 samples that had evaluable tumor-associated osteoblasts, 4 had FGFR1 expression in osteoblasts but not in PCa cells, 2 had FGFR1 in both PCa cells and osteoblasts, and in 4 samples no FGFR1 expression was found in either cell type. Of the 16 patients with tumor infiltration before treatment, 7 (43%) had tumor-infiltrated biopsies after 8 weeks of dovitinib treatment, and 3 expressed FGFR1 in PCa cells before treatment. All 3 of these patients demonstrated relative reductions in FGFR1 expression after dovitinib treatment, but we did not detect changes in p-FRS2α, p-MAPK, or p-S6K expression on IHC analysis (Table S19).

DISCUSSION

Our integrated analysis of clinical and preclinical studies supports the existence of a signaling loop between PCa and stromal cells, mediated by FGFs and FGFRs, that promotes PCa growth in bone. Our analysis also indicates that pharmacologic blockade of FGFR signaling with dovitinib disrupts this paracrine interaction to mediate an antitumor effect in preclinical models and in some men with metastatic CRPC. The effect of dovitinib on the cross-talk between PCa and bone and on the tumor microenvironment may explain why dovitinib treatment led to improvements in bone scans, lymphadenopathy, and tumor-specific symptoms without a proportional decline in PSA in some men with metastatic CRPC.

Our studies also indicate that FGFR1 is the prevalent FGFR in PCa and that dovitinib has selective antitumor activity in PDXs in which the PCa cells express high FGFR1 (MDA PCa 118b). However, even though FGFR1 was detected by IHC analysis in only 12% of PCa bone metastasis samples, approximately 26% of patients enrolled in the dovitinib trial experienced improvements in bone scans. We hypothesize that some minimum level of the FGFR transcript is needed in PCa cells to mediate the paracrine interaction between PCa cells and bone cells. This minimum level of FGFR transcript (which may not be detectable by IHC analysis) may constitute a threshold for antitumor activity of dovitinib.

Our finding that FGFR signaling blockade was associated with increased bone quality is in line with reports that adult mice lacking *Fgfr1* (in progenitor cells or in differentiated osteoblasts) have increased bone mass relative to wild-type mice (24). Cancer metastases to bone induce bone remodeling, which includes both bone formation and bone resorption processes. In PCa, bone formation predominates, resulting in a bone architecture that includes new (woven) bone in close interaction with PCa cells. It has been hypothesized that the process of bone formation prompts the generation of bone-derived factors that favor PCa growth in bone. Thus, improvements in bone quality (such as that induced by dovitinib) may counteract the bone-remodeling signals from PCa cells and inhibit tumor growth.

FGFR signals also have important roles in endothelial cells, which express high FGFR1 levels. The observed modulation of soluble VEGF and VEGFR2 by dovitinib in patients in this study is consistent with VEGFR targeting. FGFR signaling has also been reported to

mediate resistance to VEGFR targeting (25, 26), suggesting that the potent antitumor activity of dovitinib results from an enhanced antiangiogenic effect (unlike other tyrosine kinase inhibitors that target VEGFRs but do not target FGFRs) in addition to other tumor and stromal consequences of FGFR blockade (27).

Our studies, although suggesting new therapy options for men with PCa bone metastases, also have limitations. Specifically, we did not identify predictive markers of response with which to identify men who may benefit from this therapy. The identification of such markers must be a high priority project in the future. Another limitation relates to the specific mechanism of antitumor activity of dovitinib. In this regard, although our studies indicate that dovitinib blocks FGFR1 signaling, we did not identify signaling pathways downstream of FGFR1 that could be modulated by this therapy.

Our results point to a complex role of FGF signaling in PCa and suggest that variations in the biology of FGFR1-driven tumors may account for the different responses observed in our clinical trial. Clearly, a subset of patients benefits the most from dovitinib treatment, and new predictive biomarkers of response are needed. Our current model of dovitinib efficacy via FGFR blockade in bone may explain our clinical observations and could be used to guide the use of FGFR inhibition as a therapeutic option in PCa and other tumors that rely on this pathway to progress.

In summary, our clinical and preclinical studies represent a strategy for helping to elucidate the mechanism of antitumor activity in targeted drug development. Further, by using this strategy we have identified dovitinib as a clinically active drug in men with PCa bone metastases. Because responses to currently available therapies for men with PCa are usually brief, our findings address the need for additional treatment modalities or new drugs for the treatment of men with PCa metastatic to bone.

MATERIALS AND METHODS

Study design

The objective of this study was to test the effect of FGFRs blockade in PCa bone metastases. We used PCa PDXs growing in the bone of immunodeficient mice to perform *in vivo* studies. We assessed human and mouse FGFRs isoform expression in tumor bearing bones by RT-PCR with species-specific primers. We studied FGFRs expression in human PCa by RNA sequencing and FGFR1 expression and cellular localization in PCa bone metastases by IHC analyses. Antitumor activity of FGFRs blockade was tested by dovitinib, a receptor tyrosine kinase inhibitor with potent activity against FGFR and VEGFR. Treatment duration in preclinical studies was 3 weeks and 1 week. At the end of treatment we evaluated tumor volume by MRI and antiangiogenic activity by DCE-MRI. Tumor bearing bones and contralateral bones were subsequently collected and processed for histological, immunohistochemical, bone histomorphometric, RT-PCR and western blot analyses. We tested the effect of treatment on cell morphology, apoptosis, bone parameters, and expression of FGFR1, p-FRS2, or members of signaling cascades regulated by the FGF axis. We also assessed FGF23 blood levels as a pharmacodynamic biomarker of FGFR inhibition in bone during dovitinib therapy.

We also performed a Phase 2 clinical study with dovitinib in men with castrate-resistant PCa and bone metastases. Men enrolled in this trial were treated in cycles of 4 weeks. Bone marrow biopsies specimens were obtained before and after 8 weeks of treatment. Urine, serum and plasma samples were collected before and during treatment. We assessed FGFR1, p-FRS2, or members of signaling cascades regulated by the FGF axis in bone marrow biopsy specimens by IHC. We measured soluble factors in blood and urine. Treatment continued until the occurrence of clinical disease progression, toxic effects, or withdrawal of their consent to participate.

Tumor lines and osteoblast cultures

MDA PCa 2b PCa cells and MDA PCa 118b and MDA PCa 183 PCa PDXs were developed in our laboratory (13, 15, 28) and propagated as subcutaneous xenografts in 6- to 8-week-old male CB17 SCID mice (Charles River Laboratories). PC3 cells were purchased from the American Type Culture Collection. PMOs were prepared as described elsewhere (14). The PDXs were developed as described elsewhere (13, 28) with the support of the Prostate Cancer Foundation and the David H. Koch Center for Applied Research in Genitourinary Cancers at MD Anderson. All animal experiments were conducted in accordance with accepted standards of animal care and were approved by the Institutional Animal Care and Use Committee of MD Anderson.

Histologic and immunohistochemical analyses

For subcutaneous PCa PDXs, tumor samples were prepared as previously described (13). IHC analysis was done at described elsewhere (29), using antibodies against FGFR1 (Epitomics, rabbit monoclonal clone ID EPR806Y), FGFR1 (Cell Signaling, rabbit monoclonal), FRS2α (Santa Cruz Biotechnology, rabbit polyclonal sc83138), p-FRS2α (Cell Signaling, rabbit polyclonal (Tyr196)), p-p44/42 MAPK (Erk1/2) (Cell Signaling, rabbit monoclonal (Thr202/Tyr204)), p-AKT (Dako, rabbit monoclonal), p-S6K (p-S434) (AbCam, ab47379), androgen receptor (Dako, rabbit polyclonal) and cleaved caspase 3 (Cell Signaling, rabbit polyclonal [Asp175]).

PCa bone model preparation and processing

Cell preparation and bone injection were performed as previously described (13). At the end of each experiment, mice were euthanized and the dissected bones processed for histologic, micro-CT, or histomorphometric analysis or were flash-frozen and processed for RNA or protein extraction.

Real-time RT-PCR

RNA extraction and cDNA preparation were done as reported elsewhere (13). Real-time RT-PCR with SYBR-Green dye (Applied Biosystems Life Technologies) and gene-specific primers (Supplementary Table 1) were used for cDNA amplification. RT-PCR results using species-specific primers are in Supplementary Table 2

Co-culture studies, mitogenic assay, and western blot analysis

MDA PCa 118b cells were co-cultured with PMOs in a two-compartment system as previously reported (14). After 48 h of co-culture, PMO and PCa cell numbers were estimated by [^{3}H]-thymidine incorporation assay (13). Western blotting was done by standard procedures with antibodies against p-FRS2α (Cell Signaling, rabbit polyclonal [Tyr196]) or with PathScan Multiplex Western Cocktail I against p-p90RSK, p-Akt, p-p44/42 MAPK (Erk1/2), and p-S6 ribosomal protein (Cell Signaling). For western blot analysis, dissected tumor bearing bones or bone tissues were frozen in liquid nitrogen and then pulverized with stainless-steel mortar and pestle. Tissue powder was then suspended in lysis buffer containing Protease Inhibitor Cocktail (Roche Applied Science) and, if phosphorylated proteins will be investigated, also Phosphatase inhibitor Cocktail (PhosSTOP EASYpack Roche). The suspension was vortexed and then homogenized by sonication. Supernatant fraction of lysates was then used for western blot analysis. Band densities on western blots were assessed with Image J software (National Institutes of Health).

FGFR expression and copy number analysis

MDA PCa PDXs (n=17) were sequenced with an Illumina HiSeq 2000 system. Ten PCa cell lines, 19 human prostate samples derived from benign tissue adjacent to PCa, and 136 human PCa tissue specimens derived from primary and metastatic (non-bone) sites were sequenced with an Illumina Genome Analyzer II or an Illumina HiSeq 2000 system. Data from another 15 primary tumor samples were downloaded from Database of Genotypes and Phenotypes study phs000310.v1.p1 and analyzed along with the other samples.

RNA sequencing for all libraries was done according to standard Illumina protocols. Sequencing reads were mapped with TopHat version 2.0.7 software, and gene expression was quantified across genes from Ensembl version 69 using Cufflinks version 2.0.2 software. Gene expression values for the FGFR family of genes were extracted from the Cufflinks “genes.fpkm_tracking” files. All plots were created with standard R software.

Copy number analysis from exome sequencing data was performed by using an algorithm (30) with GC content correction (31). Additional details are provided in the supplementary materials.

FISH analysis

We used a FISH-based split-probe strategy to investigate the presence of genomic rearrangement in *FGFR1* (32). Bacterial artificial chromosome clones located at chromosomes 8p12-p11.23 (RP11-675F6-green) and 8p12 (RP11-513D5-red) were used to generate the dual-color break-apart FISH probes. FISH was done with bacterial artificial chromosomes with the corresponding fluorescent label on formalin-fixed, paraffin-embedded tissue sections. At least 200 nuclei were evaluated in all assays.

Treating MDA PCa 118b tumor-bearing mice with dovitinib and monitoring tumor volume and bone response

Mice with PCa cells injected into their femurs were treated daily by oral gavage with 40 or 60 mg/kg/body weight dovitinib (Novartis Pharma AG), or water used as vehicle. For the 3-week treatment protocol, drug administration started 10 days after cell injection, when we identified tumor cells in the marrow cavity by MRI. For the 7-day treatment protocol, drug administration started when changes in bone morphology were evident on X-rays, at approximately 4 weeks after cell injection. At the end of the treatment, X-ray or MRI (or both) was performed, mice were sacrificed, and tumor-bearing femurs or contralateral femurs were processed for protein or RNA extraction or were subjected to specimen micro-CT, IHC, or histomorphometric analysis of undecalcified bone. Micro-CT analysis was performed at the Small Animal Imaging Facility at MD Anderson (13). Histomorphometric analysis was performed at the Bone Histomorphometry Core Laboratory, The Bone Disease Program of Texas.

MRI

MRI was performed with a 4.7-T Biospec small-animal imaging system (Bruker Biospin). For anatomic tumor imaging, we used sagittal and axial T2-weighted fast spin-echo sequences with and without fat suppression (echo time 78 ms, repetition time 4000 ms, echo train length 12 mm, flip angle 180 mm, slice thickness 1 mm, matrix 256 × 192, 3 excitations) to delineate the tumors, and tumors were subsequently measured with Image J software (National Institutes of Health) (33). For functional imaging, we acquired a series of images of the femur in the sagittal plane with dynamic contrast-enhanced MRI before, during, and after injection of the contrast agent gadopentetate dimeglumine (Magnevist; Bayer HealthCare Pharmaceuticals) through a tail-vein catheter. We used an interleaved fast spoiled gradient echo sequence (echo time 1.4 ms, repetition time 40 ms, in-plane resolution 312 mm × 234 mm, 1-mm slice thickness, update rate approximately 3.5 s per slice package) to monitor contrast accumulation in blood vessels and tumor. Enhancement during the total time (approximately 160 s) and the initial area underneath the curve (approximately 40 s) were evaluated. The region of interest encompassing a central slice of the enhancing portion of the tumor was subtracted from the mean signal intensity before contrast injection, and the difference was divided by the number of pixels in the region of interest.

Clinical Trial (NCT00831792)

In this phase II study, chemotherapy-naïve and chemotherapy-treated men with progressive metastatic CRPC received 400–500 mg of dovitinib orally every day for 5 days, followed by a 2-day rest period. This dose and schedule was selected based on early phase I/II data demonstrating tolerability, efficacy, and inhibition of FGF signaling in patients with advanced solid tumors, including kidney cancer and melanoma (18, 19, 34). Each cycle lastsed 28 days, and radiographic response was assessed every 2 cycles. Dovitinib treatment continued until disease progression, unacceptable toxicity, or withdrawal of consent. Because clinical benefit may not be linked with changes in PSA level, disease progression was defined as any new skeletal-related event (bone scan progression, fracture, requirement for radiation), radiographic progression according to the Response Evaluation Criteria In

Solid Tumors (RECIST) system, or clinical progression as determined by the treating clinician.

Transiliac bone marrow biopsies were obtained before and after 8 weeks of treatment according to established procedures (35, 36). Written informed consent was obtained from patients before sample acquisition, and all samples were processed according to a protocol approved by the Institutional Review Board of MD Anderson.

Assessment of soluble factors after dovitinib treatment

Patients provided written institutional review board–approved informed consent for the collection of blood samples for biomarker analysis. Specimens were obtained at baseline (before treatment) and after approximately 4 or 8 weeks (or both) of treatment. Serum was prepared as described (37) and stored at −80°C until use. For analysis, VEGFR1, VEGFR2, VEGF, and VEGFC expression was measured in duplicate by using Searchlight multiplex immunoassays (Aushon Biosystems). PSA, BAP, and uNTX were measured at MD Anderson's Department of Laboratory Medicine.

FGF23 levels in the blood of mice were measured with a mouse FGF23 enzyme-linked immunosorbent assay kit (EMD Millipore Corporation).

Statistical analysis

The Wilcoxon rank-sum test was applied to compare treatment durations between groups with reduced or non-reduced levels of PSA, BAP, and uNTX. Spearman correlation coefficients were computed to evaluate the association between percentage reductions in BAP and uNTX as continuous variables and days on study. For all other analyses, two-sample *t* tests were used. *P* values less than 0.05 were considered statistically significant.

Supplementary Material

Refer to Web version on PubMed Central for supplementary material.

Acknowledgments

The authors thank Anh Hoang for technical support and Christine Wogan for editing the manuscript.

Funding. This work was supported in part by the Prostate Cancer Foundation, generous philanthropic contributions to The University of Texas MD Anderson Moon Shots Program, Cancer Center Support (Core) Grant P30 CA016672 and Prostate SPORE grant 5P50 CA140388, and the Cancer Prevention & Research Institute of Texas grant RP110555, the National Institute of Health CA96824 and the David H. Koch Center for Applied Research in Genitourinary Cancers at MD Anderson, Houston, TX.

REFERENCES

1. Carlin BI, Andriole GL. The natural history, skeletal complications, and management of bone metastases in patients with prostate carcinoma. Cancer. 2000; 88:2989. [PubMed: 10898342]
2. Loberg RD, Logothetis CJ, Keller ET, Pienta KJ. Pathogenesis and Treatment of Prostate Cancer Bone Metastases: Targeting the Lethal Phenotype. j clin oncol. 2005; 23:8232. [PubMed: 16278478]
3. Turner N, Grose R. Fibroblast growth factor signalling: from development to cancer. Nat Rev Cancer. 2010 Feb.10:116. [PubMed: 20094046]

4. Corn PG, Wang F, McKeehen W, Navone N. Targeting Fibroblast Growth Factor Pathways in Prostate Cancer. Clin Cancer Res. 2013 Sep 19.
5. Powers CJ, McLeskey SW, Wellstein A. Fibroblast growth factors, their receptors and signaling. Endocr Relat Cancer. 2000 Sep.7:165. [PubMed: 11021964]
6. Ornitz DM. FGFs, heparan sulfate and FGFRs: complex interactions essential for development. Bioessays. 2000; 22:108. [PubMed: 10655030]
7. Noriko G. Regulation of growth factor signaling by FRS2 family docking/scaffold adaptor proteins. Cancer Science. 2008; 99:1319. [PubMed: 18452557]
8. McKeehan WL, Wang F, Kan M. The heparan sulfate-fibroblast growth factor family: diversity of structure and function. Prog Nucleic Acid Res Mol Biol. 1998; 59:135. [PubMed: 9427842]
9. Acevedo VD, Gangula RD, Freeman KW, Li R, Zhang Y, Wang F, Ayala GE, Peterson LE, Ittmann M, Spencer DM. Inducible FGFR-1 Activation Leads to Irreversible Prostate Adenocarcinoma and an Epithelial-to-Mesenchymal Transition. Cancer Cell. 2007; 12:559. [PubMed: 18068632]
10. Memarzadeh S, Xin L, Mulholland DJ, Mansukhani A, Wu H, Teitell MA, Witte ON. Enhanced paracrine FGF10 expression promotes formation of multifocal prostate adenocarcinoma and an increase in epithelial androgen receptor. Cancer Cell. 2007 Dec.12:572. [PubMed: 18068633]
11. Zhang Y, Zhang J, Lin Y, Lan Y, Lin C, Xuan JW, Shen MM, McKeehan WL, Greenberg NM, Wang F. Role of epithelial cell fibroblast growth factor receptor substrate 2{alpha} in prostate development, regeneration and tumorigenesis. Development. 2008 Feb 15.135:775. 2008. [PubMed: 18184727]
12. Valta MP, Tuomela J, Bjartell A, Valve E, Vaananen HK, Harkonen P. FGF-8 is involved in bone metastasis of prostate cancer. Int J Cancer. 2008 Jul 1.123:22. [PubMed: 18386787]
13. Li ZG, Mathew P, Yang J, Starbuck MW, Zurita AJ, Liu J, Sikes C, Multani AS, Efstathiou E, Lopez A, Wang J, Fanning TV, Prieto VG, Kundra V, Vazquez ES, Troncoso P, Raymond AK, Logothetis CJ, Lin SH, Maity S, Navone NM. Androgen receptor-negative human prostate cancer cells induce osteogenesis in mice through FGF9-mediated mechanisms. J Clin Invest. 2008 Aug. 118:2697. [PubMed: 18618013]
14. Yang J, Fizazi K, Peleg S, Sikes CR, Raymond AK, Jamal N, Hu M, Olive M, Martinez LA, Wood CG, Logothetis CJ, Karsenty G, Navone NM. Prostate cancer cells induce osteoblast differentiation through a Cbfa1-dependent pathway. Cancer Res. 2001 Jul 15.61:5652. [PubMed: 11454720]
15. Roychowdhury S, Iyer MK, Robinson DR, Lonigro RJ, Wu YM, Cao X, Kalyana-Sundaram S, Sam L, Balbin OA, Quist MJ, Barrette T, Everett J, Siddiqui J, Kunju LP, Navone N, Araujo JC, Troncoso P, Logothetis CJ, Innis JW, Smith DC, Lao CD, Kim SY, Roberts JS, Gruber SB, Pienta KJ, Talpaz M, Chinnaiyan AM. Personalized oncology through integrative high-throughput sequencing: a pilot study. Sci Transl Med. 2011 Nov 30.3:111ra121.
16. Martin A, David V, Quarles LD. Regulation and function of the FGF23/klotho endocrine pathways. Physiological reviews. 2012 Jan.92:131. [PubMed: 22298654]
17. Wohrle S, Bonny O, Beluch N, Gaulis S, Stamm C, Scheibler M, Muller M, Kinzel B, Thuery A, Brueggen J, Hynes NE, Sellers WR, Hofmann F, Graus-Porta D. FGF receptors control vitamin D and phosphate homeostasis by mediating renal FGF-23 signaling and regulating FGF-23 expression in bone. Journal of bone and mineral research : the official journal of the American Society for Bone and Mineral Research. 2011 Oct.26:2486.
18. Kim KB, Chesney J, Robinson D, Gardner H, Shi MM, Kirkwood JM. Phase I/II and pharmacodynamic study of dovitinib (TKI258), an inhibitor of fibroblast growth factor receptors and VEGF receptors, in patients with advanced melanoma. Clin Cancer Res. 2011 Dec 1.17:7451. [PubMed: 21976540]
19. Angevin E, Lopez-Martin J, Lin C-C, Gschwend JE, Harzstark A, Castellano D, Soria JC, Sen P, Chang J, Shi MM, Kay A, Escudier B. Phase I Study of Dovitinib (TKI258), an Oral FGFR, VEGFR, and PDGFR Inhibitor, in Advanced or Metastatic Renal Cell Carcinoma. Clinical Cancer Research. 2013; 19:1257. [PubMed: 23339124]
20. Antonarakis ES, Carducci MA. Targeting angiogenesis for the treatment of prostate cancer. Expert opinion on therapeutic targets. 2012 Apr.16:365. [PubMed: 22413953]

21. Murakami M, Simons M. Fibroblast growth factor regulation of neovascularization. Current opinion in hematology. 2008 May.15:215. [PubMed: 18391788]

22. O'Connor JP, Jackson A, Parker GJ, Roberts C, Jayson GC. Dynamic contrast-enhanced MRI in clinical trials of antivascular therapies. Nat Rev Clin Oncol. 2012 Mar.9:167. [PubMed: 22330689]

23. Murukesh N, Dive C, Jayson GC. Biomarkers of angiogenesis and their role in the development of VEGF inhibitors. Br J Cancer. 2010 Jan 5.102:8. [PubMed: 20010945]

24. Jacob AL, Smith C, Partanen J, Ornitz DM. Fibroblast growth factor receptor 1 signaling in the osteo-chondrogenic cell lineage regulates sequential steps of osteoblast maturation. Dev Biol. 2006 Aug 15.296:315. [PubMed: 16815385]

25. Casanovas O, Hicklin DJ, Bergers G, Hanahan D. Drug resistance by evasion of antiangiogenic targeting of VEGF signaling in late-stage pancreatic islet tumors. Cancer Cell. 2005 Oct.8:299. [PubMed: 16226705]

26. Kerbel RS. Therapeutic implications of intrinsic or induced angiogenic growth factor redundancy in tumors revealed. Cancer Cell. 2005 Oct.8:269. [PubMed: 16226701]

27. Dror Michaelson M, Regan MM, Oh WK, Kaufman DS, Olivier K, Michaelson SZ, Spicer B, Gurski C, Kantoff PW, Smith MR. Phase II study of sunitinib in men with advanced prostate cancer. Ann Oncol. 2009 May.20:913. [PubMed: 19403935]

28. Navone NM, Olive M, Ozen M, Davis R, Troncoso P, Tu SM, Johnston D, Pollack A, Pathak S, von Eschenbach AC, Logothetis CJ. Establishment of two human prostate cancer cell lines derived from a single bone metastasis. Clin Cancer Res. 1997 Dec.3:2493. [PubMed: 9815652]

29. Efstathiou E, Titus M, Tsavachidou D, Tzelepi V, Wen S, Hoang A, Molina A, Chieffo N, Smith LA, Karlou M, Troncoso P, Logothetis CJ. Effects of abiraterone acetate on androgen signaling in castrate-resistant prostate cancer in bone. J Clin Oncol. 2012 Feb 20.30:637. [PubMed: 22184395]

30. Lonigro RJ, Grasso CS, Robinson DR, Jing X, Wu YM, Cao X, Quist MJ, Tomlins SA, Pienta KJ, Chinnaiyan AM. Detection of somatic copy number alterations in cancer using targeted exome capture sequencing. Neoplasia. 2011 Nov.13:1019. [PubMed: 22131877]

31. Robinson DR, Wu YM, Kalyana-Sundaram S, Cao X, Lonigro RJ, Sung YS, Chen CL, Zhang L, Wang R, Su F, Iyer MK, Roychowdhury S, Siddiqui J, Pienta KJ, Kunju LP, Talpaz M, Mosquera JM, Singer S, Schuetze SM, Antonescu CR, Chinnaiyan AM. Identification of recurrent NAB2-STAT6 gene fusions in solitary fibrous tumor by integrative sequencing. Nature genetics. 2013 Feb.45:180. [PubMed: 23313952]

32. Han B, Mehra R, Dhanasekaran SM, Yu J, Menon A, Lonigro RJ, Wang X, Gong Y, Wang L, Shankar S, Laxman B, Shah RB, Varambally S, Palanisamy N, Tomlins SA, Kumar-Sinha C, Chinnaiyan AM. A fluorescence in situ hybridization screen for E26 transformation-specific aberrations: identification of DDX5-ETV4 fusion protein in prostate cancer. Cancer Res. 2008 Sep 15.68:7629. [PubMed: 18794152]

33. Yang D, Han L, Kundra V. Exogenous gene expression in tumors: noninvasive quantification with functional and anatomic imaging in a mouse model. Radiology. 2005 Jun.235:950. [PubMed: 15914480]

34. Kim KB, Saro J, Moschos SS, Hwu P, Tarhini AA, Hwu W, Jones G, Wang Y, Rupani H, Kirkwood JM. A phase I dose finding and biomarker study of TKI258 (dovitinib lactate) in patients with advanced melanoma. J Clin Oncol. 2008; 26

35. Mathew P, Thall PF, Bucana CD, Oh WK, Morris MJ, Jones DM, Johnson MM, Wen S, Pagliaro LC, Tannir NM, Tu S-M, Meluch AA, Smith L, Cohen L, Kim S-J, Troncoso P, Fidler IJ, Logothetis CJ. Platelet-Derived Growth Factor Receptor Inhibition and Chemotherapy for Castration-Resistant Prostate Cancer with Bone Metastases. Clin Cancer Res. 2007 Oct 1.13:5816. 2007. [PubMed: 17908974]

36. Logothetis CJ, Wen S, Molina A, Chieffo N, Smith LA, Troncoso P, E E. Identification of an androgen withdrawal responsive phenotype in castrate resistant prostate cancer (CRPC) patients (pts) treated with abiraterone acetate (AA). J Clin Oncol. 2008; 26

37. Zurita AJ, Jonasch E, Wang X, Khajavi M, Yan S, Du DZ, Xu L, Herynk MH, McKee KS, Tran HT, Logothetis CJ, Tannir NM, Heymach JV. A cytokine and angiogenic factor (CAF) analysis in

plasma for selection of sorafenib therapy in patients with metastatic renal cell carcinoma. Ann Oncol. 2012 Jan.23:46. [PubMed: 21464158]

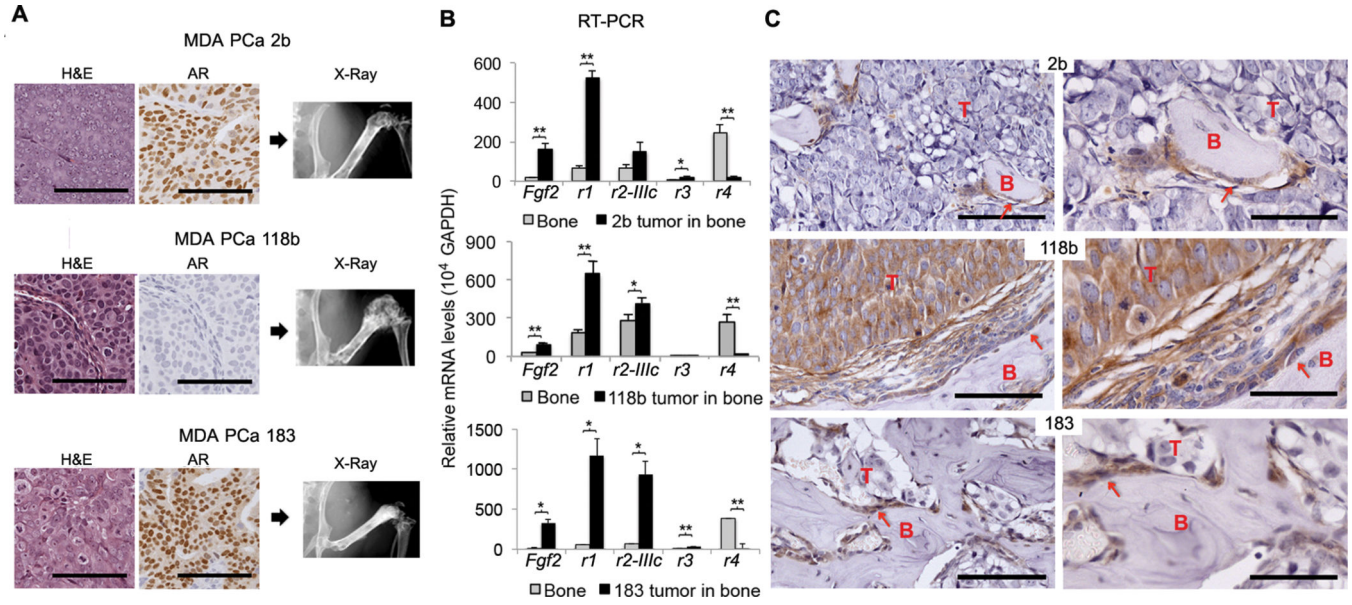

Fig. 1.

Expression of FGF and FGFR in human PCa cells and host bones. (**A**) H&E-stained tissue sections (left) and immunohistochemical stains for androgen receptor (AR; middle) in MDA PCa 2b (2b), MDA PCa 118b (118b), and MDA PCa 183 (183) cells grown subcutaneously in SCID mice. Scale bar 100 microns. Radiographs of mouse hemi-pelvises and rear limbs injected intrafemorally with PCa cells (right). (**B**) mRNA expression of *Fgf2*, *Fgfr1* (*r1*), *Fgfr2-IIIc* (*r2IIIc*), *Fgfr3* (*r3*), and *Fgfr4 (r4*) in mouse femurs with or without tumors using mouse-specific primers. Femurs with tumors expressed significantly more *Fgf2* and *Fgfr1* than femurs without tumors for all PCa PDXs tested. **P*<0.05, ***P*<0.005, two-tailed paired *t* test. Error bars indicate standard error of the mean (SEM). (n=6 mice per PDX line for 2b and 118b and n=5 mice for 183 PDX line) (**C**) IHC staining for FGFR1 in the bones of mice. Scale bar 100 μm (left panels) and 50 μm (right panels). T, tumor; B, bone; arrows indicate osteoblasts. FGFR1 was detected by IHC analysis in tumor-associated osteoblasts in all three PCa PDXs, but in PCa cells only in the 118b PDX.

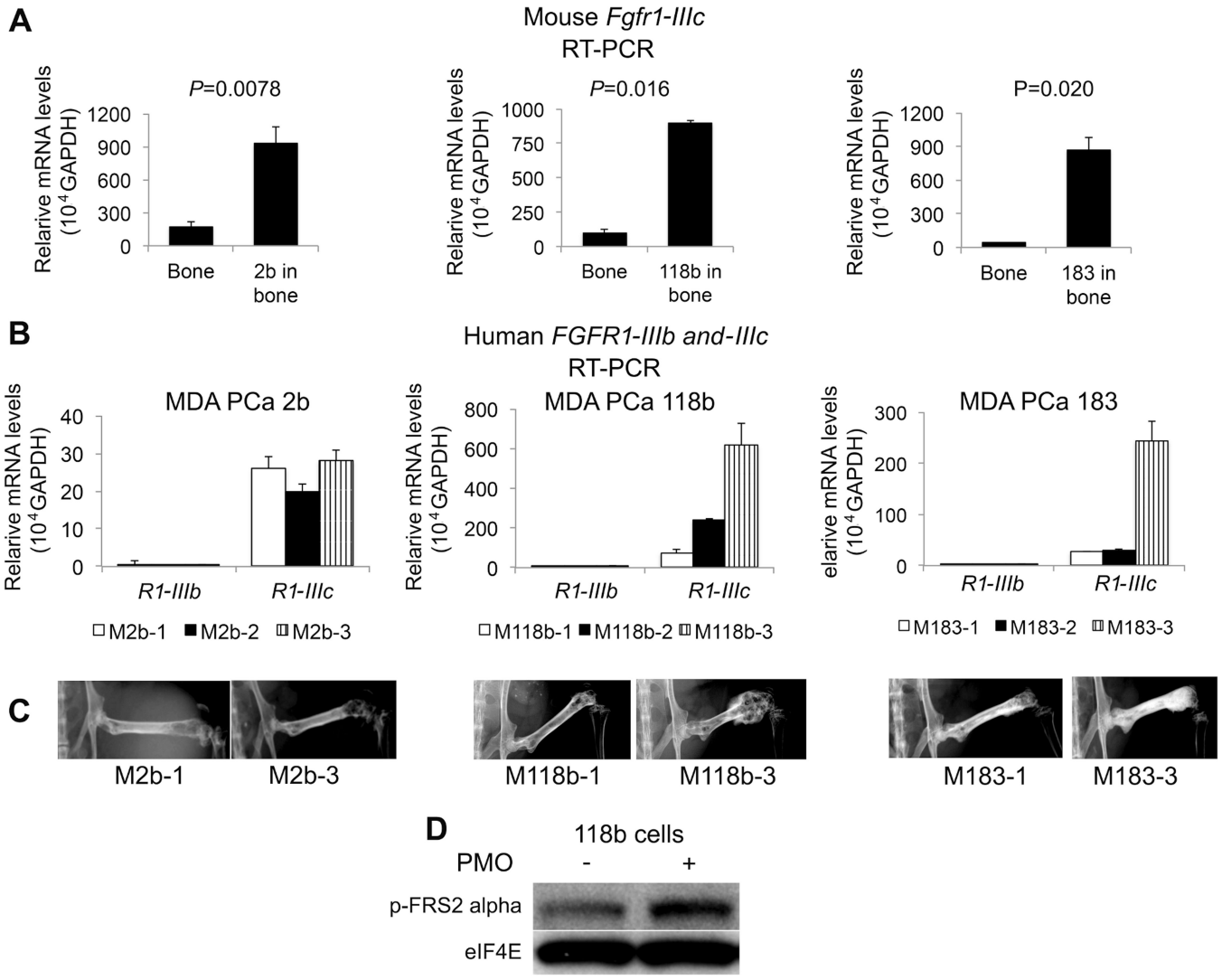

Fig 2.

FGFR1-IIIc expression in human PCa bone tumors and host bones. (**A**) Relative *Fgfr1-IIIc* mRNA expression in mouse femurs with or without MDA PCa 2b (2b), MDA PCa 118b (118b), and MDA PCa 183 (183) tumors using mouse-specific primers. Femurs with tumors expressed significantly more *Fgfr1-IIIc* than femurs without tumors for all PCa PDXs tested. *P* values are from two-tailed paired *t* tests; error bars indicate standard error of the mean (SEM). (n=6 mice per PDX line for 2b and 118b and n=3 mice for 183 PDX line). (**B**) Relative mRNA expression of *FGFR1-IIIb* (*R1-IIIb*) and *FGFR1-IIIc (R1-IIIc*) in tumor-bearing femurs from three mice per PDX group (2b, 118b, and 183 cells). Error bars indicate standard error of the mean (SEM). All PCa PDXs tested expressed between 50 and 100 times more *FGFR1-IIIc* than *FGFR1-IIIb*. (**C**) Radiographs of mouse hemi-pelvises and rear limbs injected intrafemorally with PCa cells illustrate that tumor burden (indicated by increased bone density and bulky areas at the site of bone injection of PCa cells) correlates with *FGFR1-IIIc* levels as shown in (**2B**). (**D**) Western blot analysis of MDA PCa 118b cells grown alone or in co-culture with primary mouse osteoblasts (PMOs). Phosphorylated (p-)

FRS2α expression was higher in MDA PCa 118b cells grown in co-culture than in cells grown alone. eIF4E was used as a loading control.

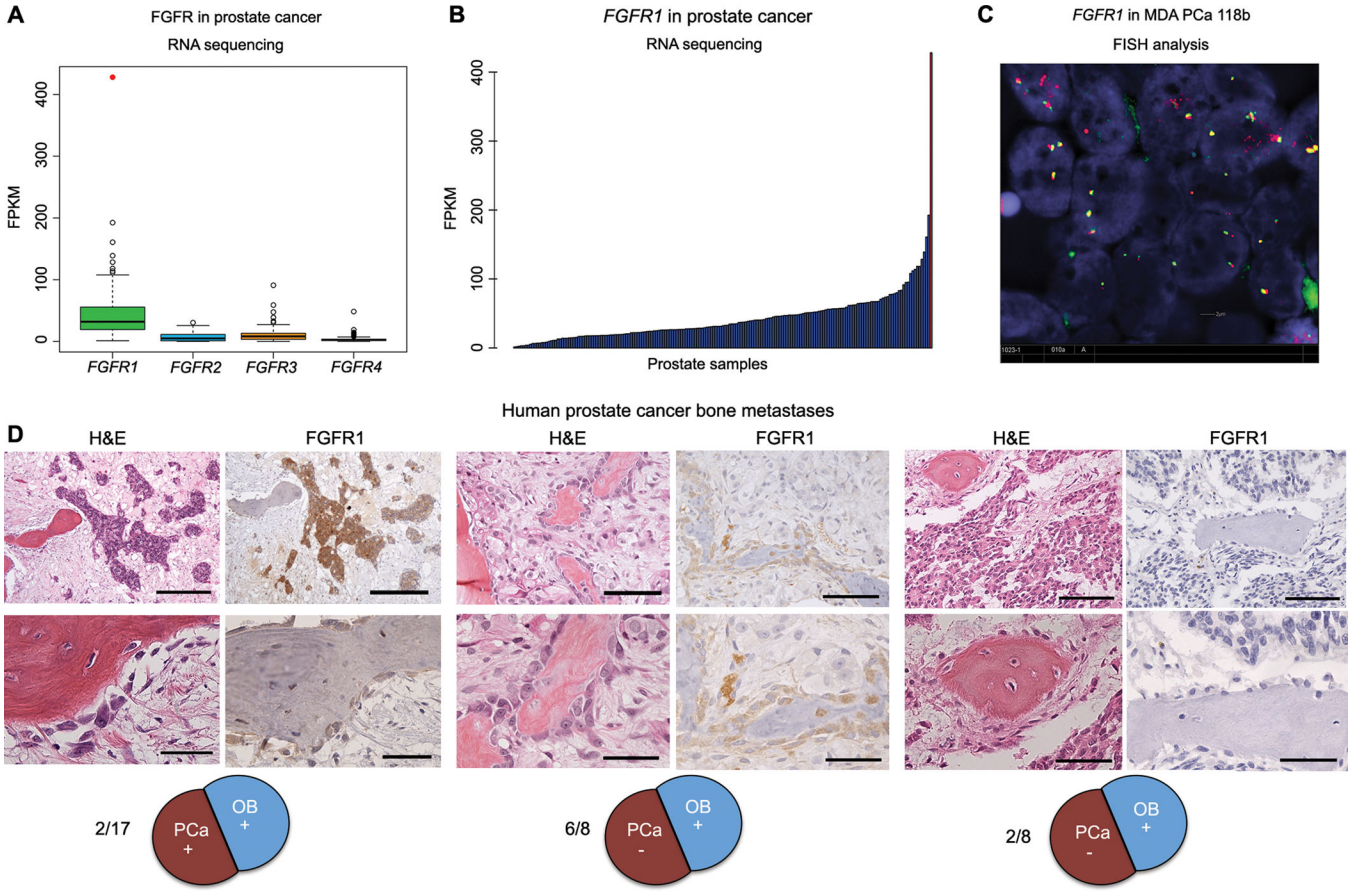

Fig. 3.

FGFR gene family expression in 183 prostate tissues, including PDXs, cell lines, and clinical tissue samples. (**A**) Boxplots showing RNA sequencing gene expression values (in reads per kilobase per million [RPKM]) for *FGFR* family genes in 17 PDXs, 10 PCa cell lines, 19 prostate tissues derived from benign tissue adjacent to PCa, and 136 PCa tissue specimens derived from primary and metastatic (non-bone) sites. The outlier expression of *FGFR1* in PDX sample MDA PCa 118b is shown as a red dot. (**B**) Bar graph of *FGFR1* expression in the 183 samples presented in (**A**). The rightmost bar represents MDA PCa 118b. (**C**) Fluorescence in situ hybridization (FISH) split-signal assay of *FGFR1* in formalin-fixed, paraffin-embedded tissue sections of the MDA PCa 118b PDX was performed with bacterial artificial chromosome probes RP11-675F6 (for the 5' portion; green) and RP11-513D5 (for the 3' portion; red). At least 200 nuclei were evaluated. (**D**) FGFR1 expression in human PCa bone metastases was assayed with FGFR1 antibody (Epitomics). Representative microphotographs of H&E staining and IHC staining with anti-FGFR1 antibody in tissue sections of human PCa bone metastases. Left, positive FGFR1 staining in PCa cells and osteoblasts (2 of 17); scale bars, upper panel 200 μm, lower panel 50 μm. Middle, FGFR1 staining in osteoblasts only (6 of 8); scale bars, upper panel 100 μm, lower panel 50 μm. Right, negative FGFR1 staining (2 of 8); scale bars, upper panel 100 μm, lower panel 50 μm.

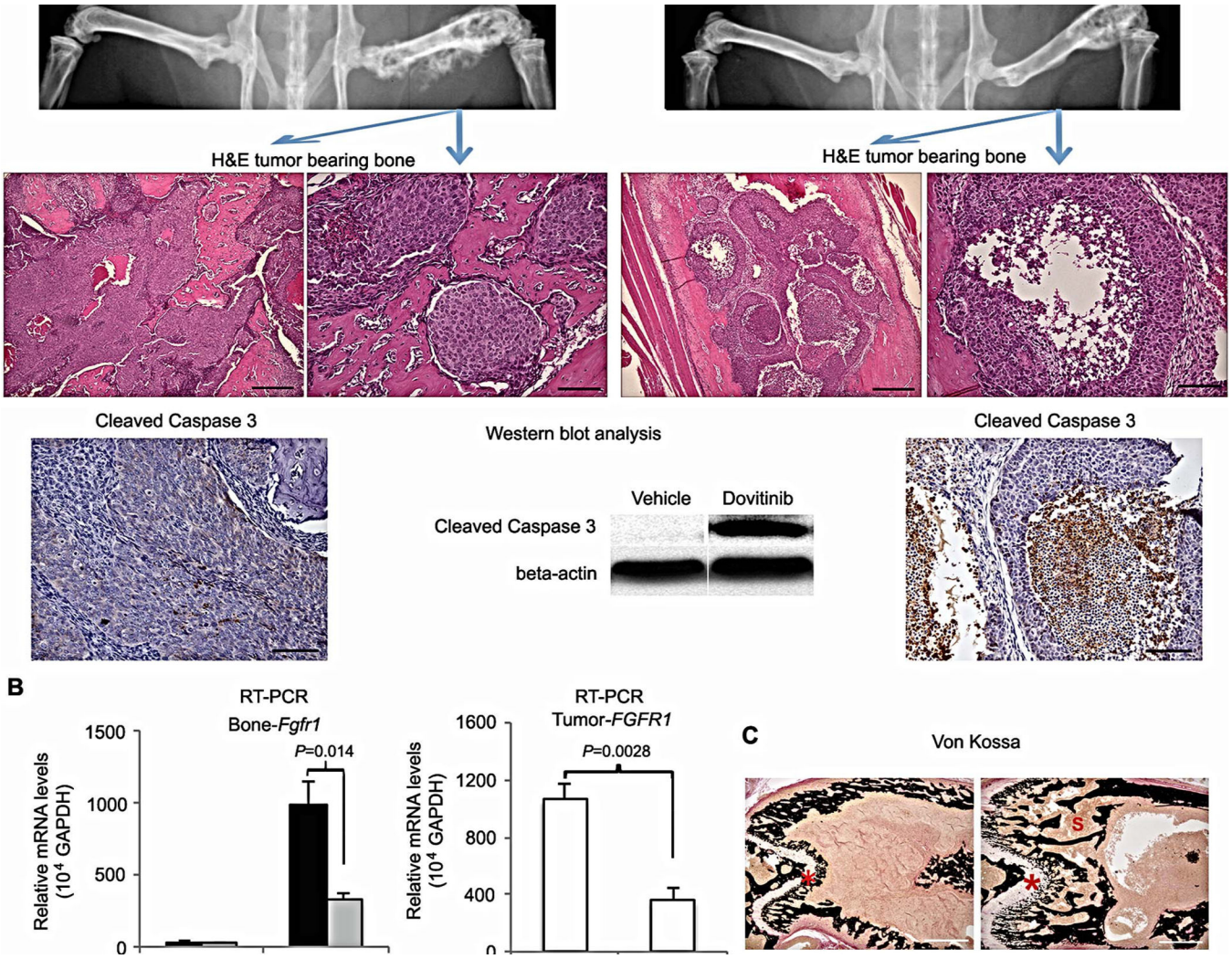

Fig. 4.

Effects of dovitinib treatment on mice with MDA PCa 118b tumor-bearing bones. (**A**) Mice treated without dovitinib (vehicle; left) or with dovitinib for 7 days (right). Top: Representative radiographs of pelvis and rear limbs. Blue arrows indicate MDA PCa 118b–bearing femurs illustrated in H&E-stained sections (middle). In the treated mouse, central areas of the tumor were empty or exhibited necrotic-like cells. Scale bars 200 μm (left in vehicle and dovitinib panels) and 50 μm (right in control and dovitinib panels). Bottom: Activated (cleaved) caspase 3 was not detected by IHC staining (left) or western blotting (center) in the tumors of vehicle-treated mice, but it was detected by IHC staining (right) and western blotting (center) in the tumors of dovitinib-treated mice. Scale bar 100 microns. (**B**) Relative expression of *Fgfr1* in mouse femur (with and without tumors) (left) and *FGFR1* in tumor-bearing femurs (right) using mouse- and human-specific primers. RNA was isolated from the contralateral (sham-injected) femurs and the MDA PCa 118b–bearing femurs of control and dovitinib-treated mice. Human *FGFR1* mRNA expression in MDA PCa 118b bone tumors was lower in dovitinib-treated mice than in the controls. Error bars indicate SEM; *P* values are from two-tailed *t* tests (n=4 mice per PDX). (**C**) Representative

cross-sectional images of undecalcified bone stained with von Kossa (black). The growth plate, primary and secondary spongiosa in the femur of the dovitinib-treated mouse were larger than in the controls. Scale bar 500 μm. *growth plate; E, primary and secondary spongiosa.

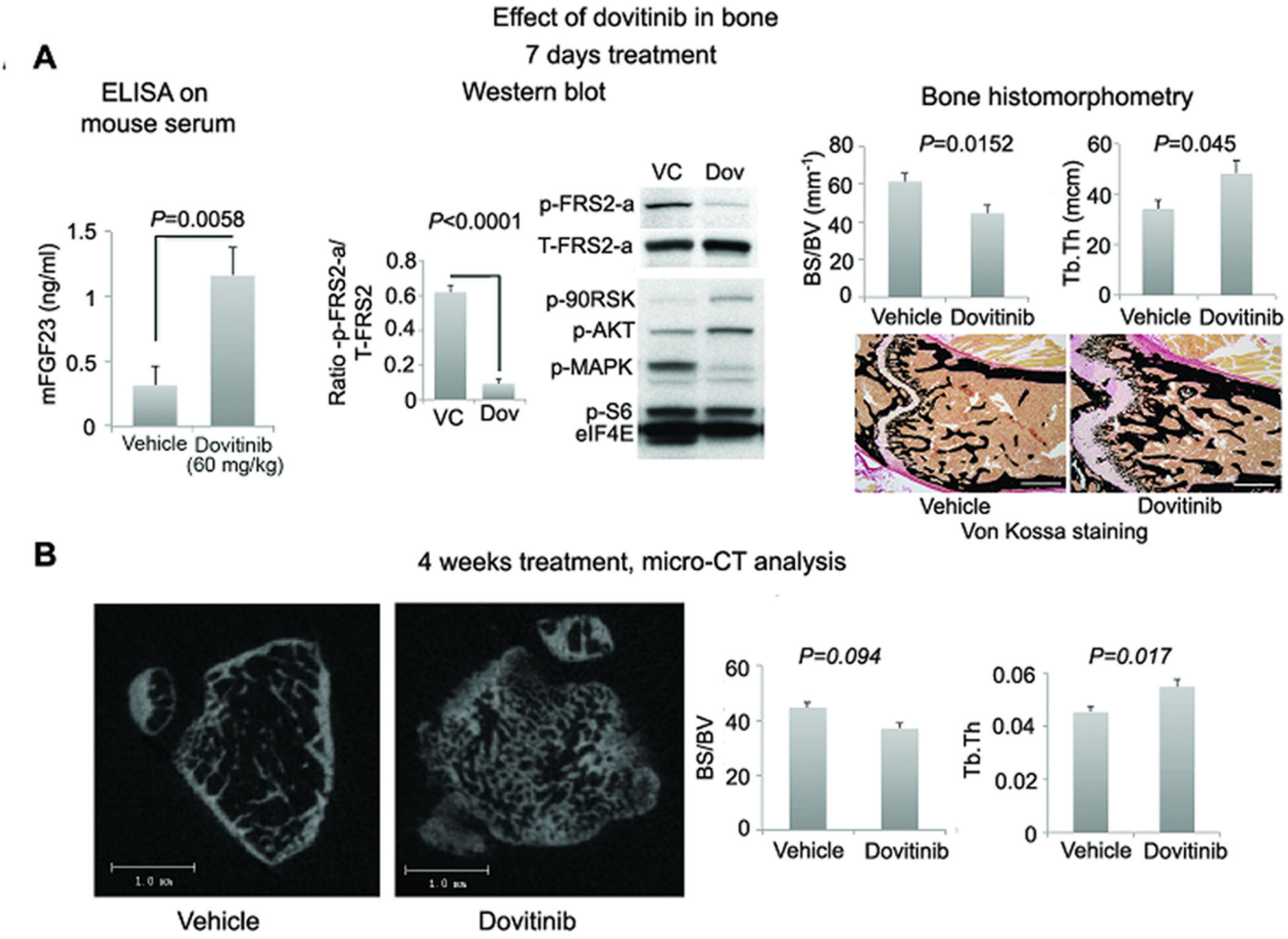

Fig. 5.

FGFR activity in bone and bone quality in dovitinib-treated mice. (**A**) Left: FGF23 levels in blood of mice with MDA PCa 118b bone tumors were higher in dovitinib-treated mice (n=7) than in controls (n=8). Center: Mean ratio of p-FRS2α/total-FRS2α (T-FRS2α) western blot band densities of contralateral (non-tumorous) femurs of mice with MDA PCa 118b bone tumors (4 vehicle- and 4 dovitinib-treated mice) and representative western blot image of the femur of 1 vehicle- and 1 dovitinib-treated mice. These results illustrate that dovitinib led to a reduction in p-FRS2α expression. Right: findings from bone histomorphometry of femurs of contralateral (non-tumorous) femurs of mice with MDA PCa 118b bone tumors (n=8 vehicle- and 8 dovitinib-treated mice), and representative photomicrographs of undecalcified bone stained with von Kossa. Bone histomorphometry indicated that dovitinib reduced the ratio of bone surface to bone volume (BS/BV) and increased trabecular thickness (Tb.Th.) in treated mice, suggesting improved bone quality. Scale bar, 500 μm. (**B**) Micro-CT analysis of the femur of non-tumor bearing mice treated with dovitinib for 4 weeks. Left: Two-dimensional slices. Right: bone parameters were similar to bone histomorphometric analysis outlined in Fig. 5A **right** (n=8 vehicle and 8 dovitinib treated mice). *P* values are from two-tailed *t* tests; error bars indicate SEM.

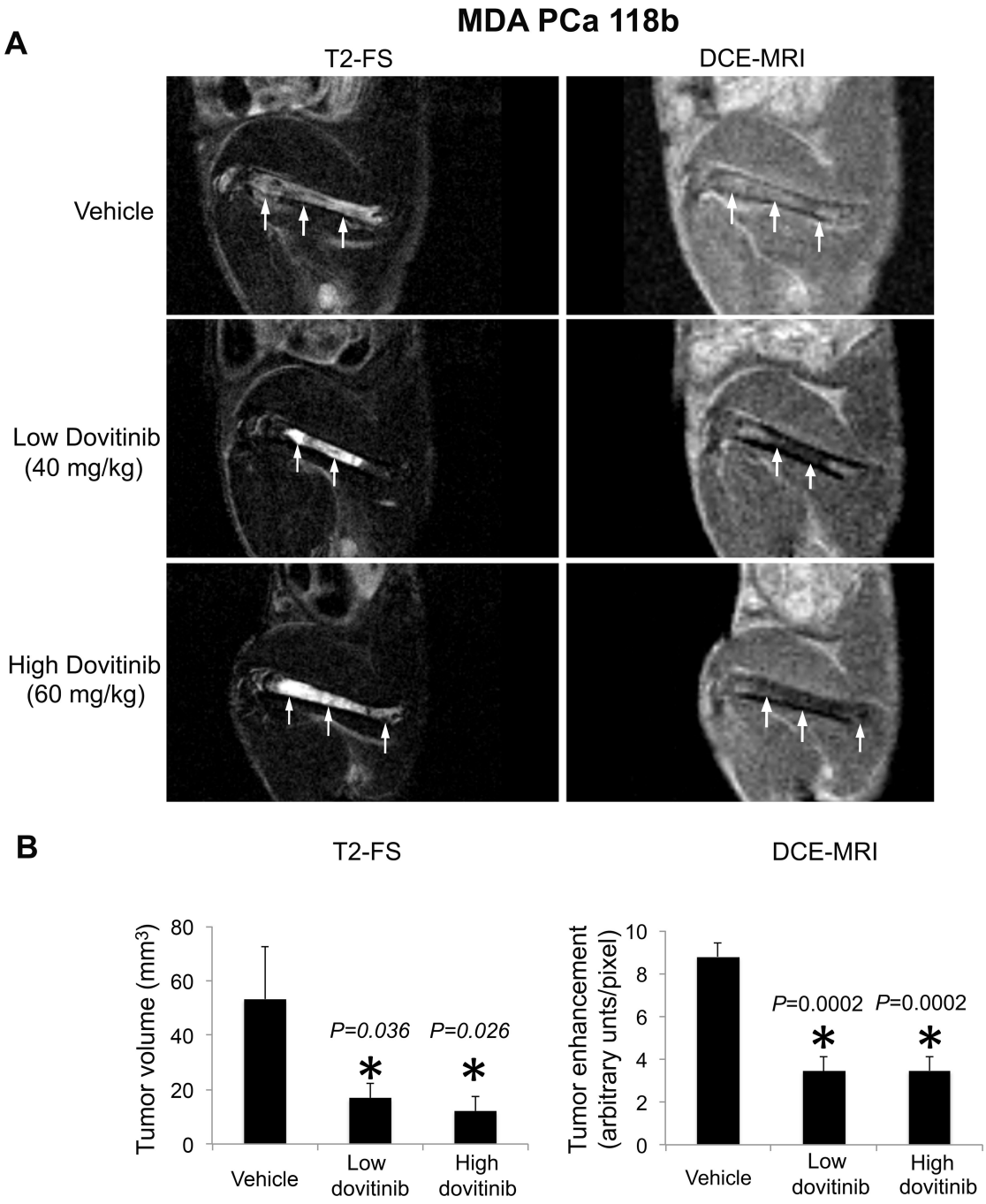

Fig. 6.

Effect of dovitinib on tumor angiogenesis in mice. (**A**) Representative sagittal MR images of MDA PCa 118b–bearing femurs in control and dovitinib-treated mice acquired with a 4.7-T scanner using a T_2-weighted fast spin (T_2-FS) echo sequence with fat suppression (left) or dynamic contrast-enhanced (DCE) MRI (right) at 7 days after treatment with vehicle (top), low-dose (middle), or high-dose dovitinib (bottom). Arrows indicate tumor, which appears as areas of increased signal on T_2-weighted images; on the contrast-enhanced sequence, less enhancement suggests less tumor vascularity and more enhancement more tumor

vascularity. (**B**) After 7 days of treatment with low or high dovitinib doses, tumor volume (left panel) and contrast enhancement (right panel) decreased compared with vehicle. *P* values in left panel are for each treatment compared with vehicle. *P* values are from one-tailed *t* tests; n=12 for control and high dovitinib and n=13 for low dovitinib. *P* values in the right panel are for each treatment compared with vehicle in two-tailed *t* tests n=6 per group. Error bars indicate SEM.

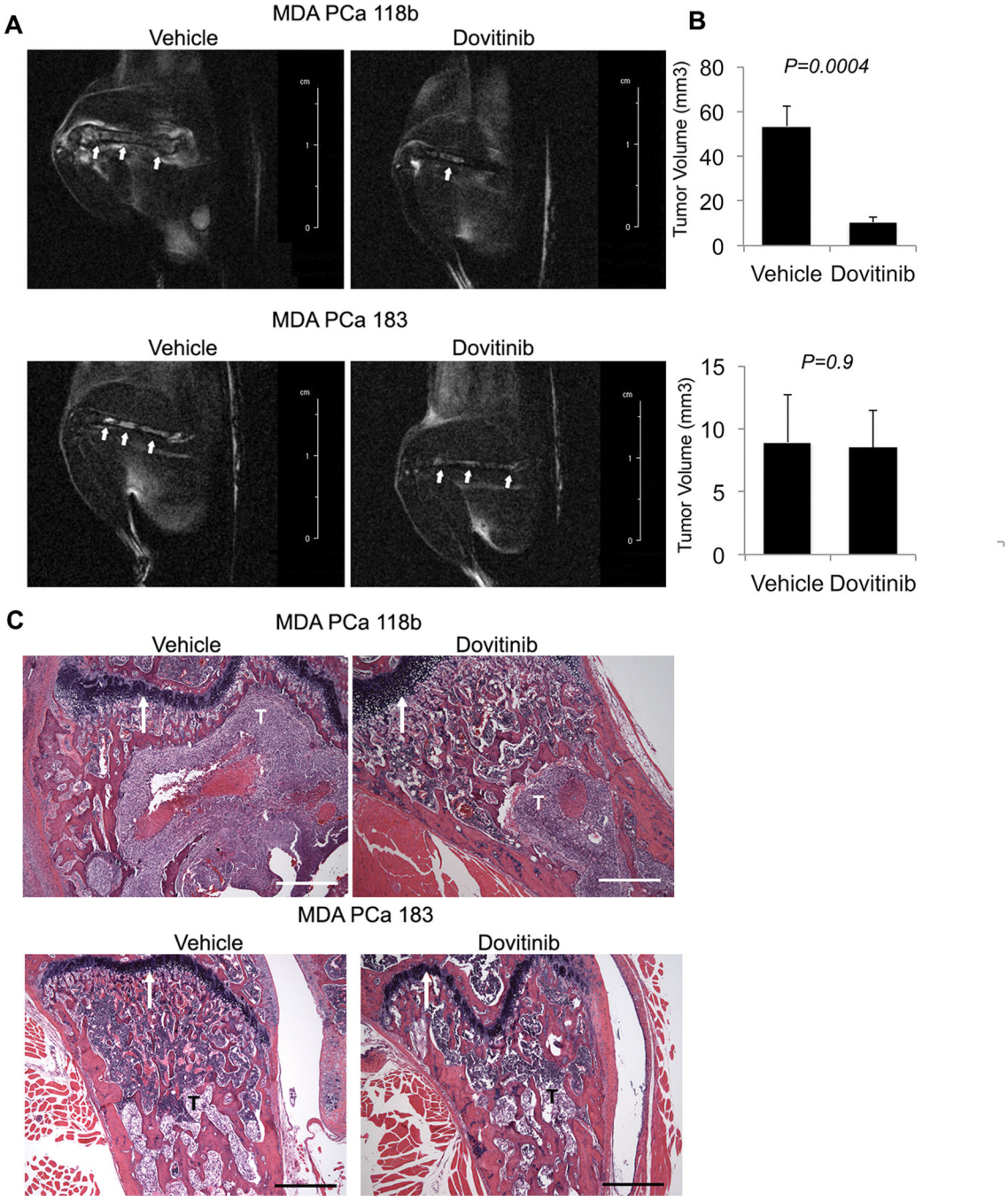

Fig. 7.

Effect of dovitinib in PCa PDXs with high and low *FGFR1* gene expression. (**A**) Representative sagittal MR images of MDA PCa 118b– and MDA PCa 183–bearing femurs in control and dovitinib-treated mice. The images were acquired with a 4.7-T scanner using a T2-weighted fast-spin echo sequence with fat suppression 3 weeks after treatment with vehicle (left) or dovitinib (right). Arrows indicate tumor. (**B**) After 3 weeks of treatment with dovitinib, tumor volume measured by MRI was smaller than in vehicle-treated mice, but only for mice bearing MDA PCa 118b tumors and not for MDA PCa 183 tumors. *P*

values are versus treatment with vehicle. Error bars indicate SEM. (**C**) Longitudinal sections of MDA PCa 118b– and MDA PCa 183–bearing femurs stained with H&E. The large tumor area in the vehicle-treated MDA PCa 118b–bearing mouse occupies most of the region captured by the 5× lens. The tumor area is much smaller in the dovitinib-treated MDA PCa 118b-bearing mouse, which supports the antitumor effect of dovitinib in this PDX. By contrast, tumor areas in vehicle- and dovitinib-treated MDA PCa 183–bearing mice are similar and reflect the lack of antitumor activity in the MDA PCa 183 PDX. All images were taken with the growth plate used as reference (white arrows). T, tumor. Scale bar, 500 μm; *P* values are from two-tailed *t* tests. n=8 for each PDX line and each group. Error bars indicate SEM.

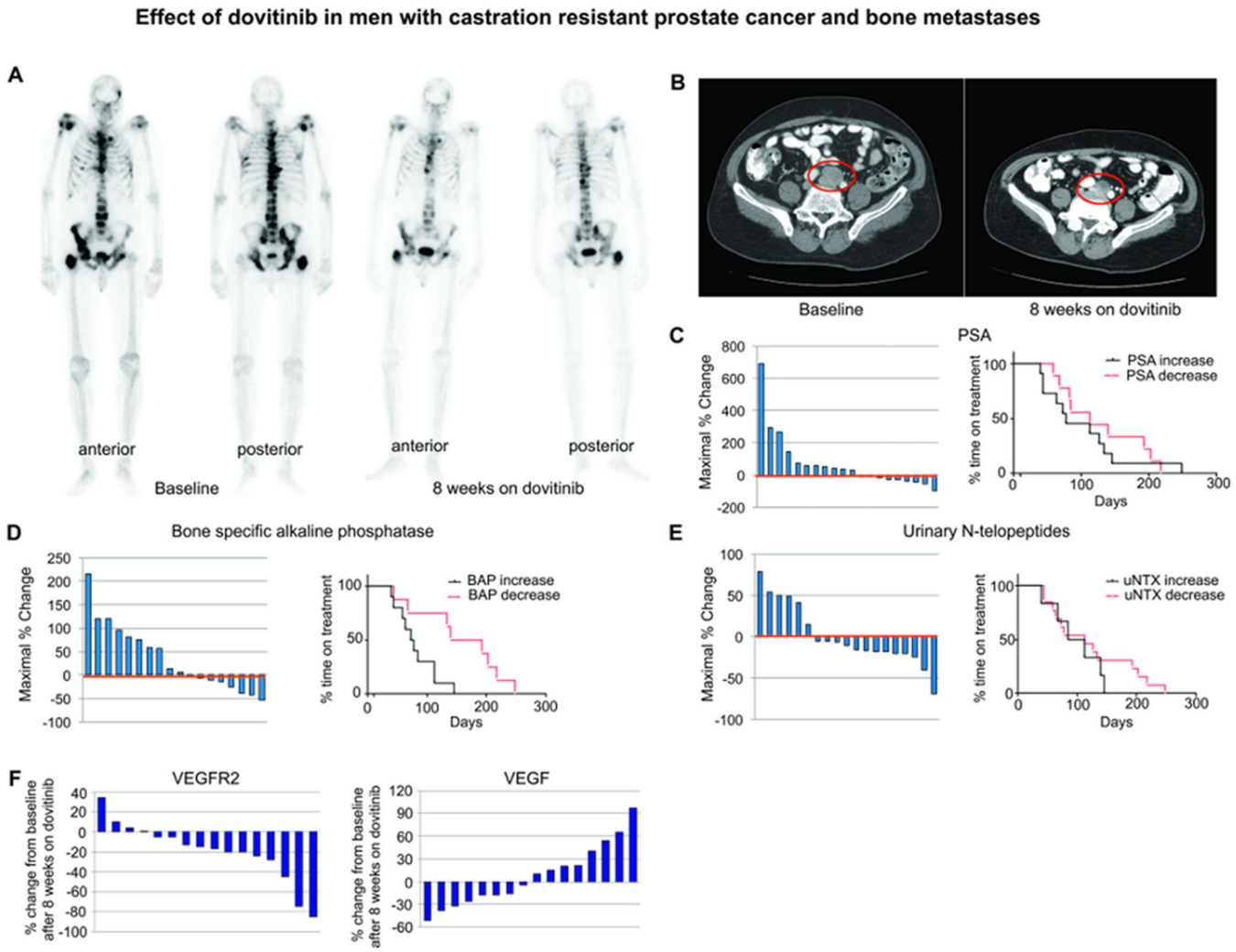

Fig. 8.

Effect of dovitinib on men with CRPC and bone metastases. (**A**) Bone scans of a patient before and after dovitinib treatment. Anterior and posterior views are shown before treatment and at 8 weeks. (**B**) CT scans of the abdomen and pelvis of another patient before (left) and at 8 weeks (right) of dovitinib treatment. Note interval improvement in lesions in both patients. (**C–E**) Waterfall plots (showing maximum % change from baseline) and median duration of treatment based on change in plasma PSA (C), BAP (D), and uNTx (E) after 8 weeks of dovitinib therapy. (**F**) Waterfall plot of human VEGFR2 and VEGF plasma concentrations. Values reflect % changes of VEGFR2 and VEGF plasma concentrations after 8 weeks of dovitinib treatment compared to baseline.

Table 1

Summary of response in evaluable patients (>1 cycle dovitinib therapy)

			REASON OFF TREATMENT		
BEST RESPONSE	**No. of Patients**	**Median Treatment Duration, weeks (range)**	**Progression**	**Toxicity[1]**	**Other[2]**
Progression	4 (17%)	8 (6–8)	4	–	–
Stable Disease	13 (57%)	11.7 (6–31)	6	4	3
Partial Response	5 (22%)	19.9 (10–35)	3	1	1
Complete Response	1 (4%)	24	–	–	1
Total	23		13	5	5

[1] Toxicities are listed in Table S18

[2] Includes 1 patient who withdrew and 1 cerebrovascular accident unrelated to therapy

Sci Transl Med. Author manuscript; available in PMC 2015 September 03.